Time Efficient Modeling of the Vibrational Behaviour of Permanent-Magnet Synchronous Machines with Non-uniform Air Gap Shape

Kevin Jansen, Marius Franck, Sebastian Mönninghoff and Kay Hameyer
Institute of Electrical Machines (IEM)
RWTH Aachen University
Aachen, Germany
kevin.jansen@iem.rwth-aachen.de

***Abstract*—The simulation of electrical machines requires efficient methods to characterize among other properties its vibrational behavior. In particular, when considering geometrical asymmetries, the accuracy of analytical approaches is often not sufficient. Magnetic circuit simulations by finite-element analysis (FEA) more accurately calculate force excitations and noise emissions, but are highly time consuming. As a compromise between speed and accuracy, semi-analytical approaches are useful to estimate the impact of the relevant parasitic effects such as static and dynamic eccentricity and axial bending. In this work, a conformal mapping approach is used to consider non-uniform air gap shapes in symmetrical FEA. A numerical modal analysis is conducted to find modal parameters of the structure. The structural dynamic vibration of the machine is modeled by modal superposition using the principal component analysis. A state space model is parameterized using these approaches and the structural dynamic transfer path from stator teeth to stator housing is studied. The aim of this work is to provide a methodology for the time efficient modeling of acoustic emissions due to electromagnetic excitations in permanent magnet synchronous machines.**

***Index Terms*—Conformal Mapping, Rotor Eccentricity, NVH**

I. Introduction

The acoustic requirements of electrical traction drives steadily increase in automative applications. Tonal noises excited by the magnetic air gap field of electrical machines are crucial and they have to be considered in the design process. The electromagnetic force waves required for torque generation include spatial and time harmonics of higher orders and cause vibration of the structure of the machine [1]. Parasitic effects of rotor misalignment effects, such as static and dynamic eccentricity as well as axial bending excite additional harmonic orders in the magnetic air gap force spectrum. Additionally, rotor eccentricity effects include implications for the service life time of the machine, such as increased bearing load due to unbalanced magnetic pull [2]. Since three dimensional, numerical calculations based on finite element analysis of multi-pole machines are time consuming in both a mechanical and an electromagnetic context, semi-analytical approaches for electromagnetic force calculation and structural dynamic analysis are approriate to study the vibrational behaviour of electrical machines. In past work, conformal mapping has been applied to model the slotting effect of salient pole synchronous machines [3] and surface mounted permanent magnet synchronous machines [4]. Eccentricity effects have been modeled in finite element simulations using non-conformal mapping [5]. In this paper, a conformal mapping approach to calculate the magnetic flux density due to rotor misalignment from a symmetrical finite element solution is proposed. Based on the magnetic air gap flux density the electromagnetic force excitations in the air gap are calculated. A modal analysis of the machine under study is performed and a state space approach for structrucal dynamical analysis is presented. The vibrational behavior of an examplary machine with different configurations of rotor displacement is studied and frequencies with increased noise emission are identified. Finally, conclusions are drawn and an outlook for the future research is given.

II. Methodology

A. Conformal Mapping of Rotor Eccentricity

In order to calculate the influence of rotor eccentricity on the magnetic air gap flux density of the machine a conformal mapping approach is applied. The domain of a regular annulus representing the air gap between rotor and stator is mapped to the air gap domain between a concentric outer circle (stator) and an eccentric inner circle (rotor). A complex Moebius transformation of the form

$$z(w) = R_\mathrm{S} \frac{\beta R_\mathrm{S} + w}{R_\mathrm{S} + \beta w} \tag{1}$$

is chosen as the inverse of the moebius transformation from the eccentric to the concentric geometry presented in [6], where R_S is the inner stator radius and z and w are points in the eccentric and concentric air gap domains, respectively.

The remaining parameter β is obtained by applying the boundary conditions

$$w(-R_\mathrm{R}) = z(-R_\mathrm{R} + d_\mathrm{Ecc}) \tag{2}$$
$$w(R_\mathrm{R}) = z(R_\mathrm{R} + d_\mathrm{Ecc}) \tag{3}$$

The rotor with the outer radius R_R is shifted along the real axis by the eccentricity amplitude d_Ecc. In figure 1 the transformation of an examplary machine geometry is plotted.

The influence of the eccentric rotor position on the magnetic field in the airgap of the machine is modeled by the complex relative permeance function λ_Ecc. This permeance function is obtained from the partial derivative of the transformation function:

$$\lambda_\mathrm{Ecc} = \frac{\delta z}{\delta w} = R_\mathrm{S}^2 \frac{\beta^2 - 1}{(R_\mathrm{S} + \beta w)^2} \tag{4}$$

Varying amplitudes of eccentricity along the axial length of the machine are modeled by using a multislice approach. The position of the eccentricity, i.e. the angular position φ of minimal airgap width, is realized by rotating the relative permeance function λ_Ecc accordingly:

$$\lambda_{\mathrm{Ecc},\varphi}(\alpha, \varphi) = \lambda_\mathrm{Ecc}(\alpha) \cdot e^{\mathrm{j}\varphi} \tag{5}$$

B. Magnetic Flux Density and Force Density Calculation

The magnetic flux density solution of the non-eccentric geometry B_Sym is obtained by Finite-Element-Analysis (FEA). In an earlier work, slotting effect in electrical machines is considered by multiplication of the slotless magnetic flux density with the complexly conjugated, relative permeance function [7]. Accordingly, the magnetic flux density in the air gap of the eccentric geometry B_Ecc is calculated by:

$$B_\mathrm{Ecc} = B_\mathrm{Sym} \cdot \lambda_\mathrm{Ecc}^* \tag{6}$$

Due to magnetic saturation not being considered in the conformal mapping approach, the relative permeance function overestimates the eccentricity effect. The original saturation state is implicitly known from the symmetrical simulation. In figure 2 the relative permeance function in no-load operation calculated from FEA is illustrated. For this, the radial and tangential components B_Rad and B_Tan of the magnetic air gap flux density are simulated for the cases of an eccentric and concentric rotor. The static eccentricity equals $d_\mathrm{Ecc} \approx 28.5\%$ of the nominal airgap width. The relative permeance function is calculated to

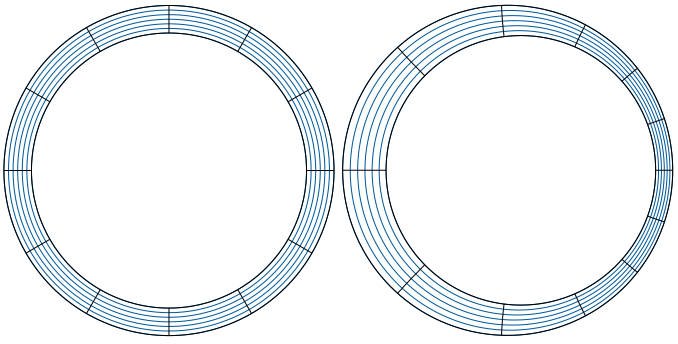

Fig. 1. Air gap shape in original w-Domain (left) and transformed to the z-Domain (right).

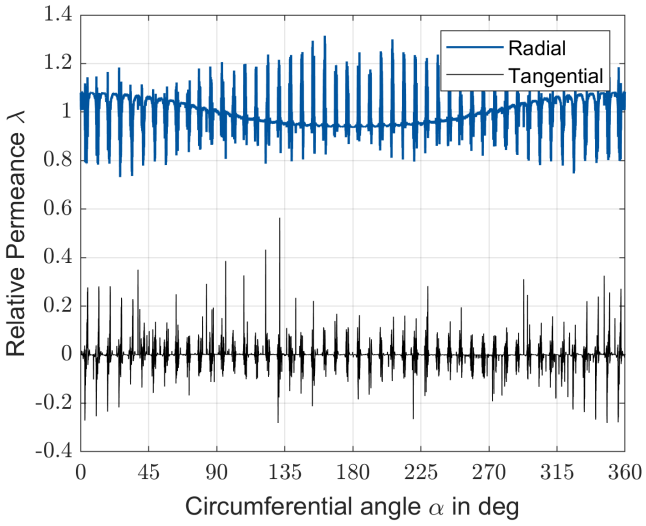

Fig. 2. Radial and tangential components of the relative permeance function calculated from FEA ($\frac{d_\mathrm{Ecc}}{\delta_\mathrm{N}} = 0.285, \varphi_\mathrm{Ecc} = 0$).

$$\lambda_\mathrm{Ecc} = \frac{B_\mathrm{Rad,Ecc} + \mathrm{j} \cdot B_\mathrm{Tan,Ecc}}{B_\mathrm{Rad,Sym} + \mathrm{j} \cdot B_\mathrm{Tan,Sym}} \tag{7}$$

and averaged over all rotational angles in order to minimize the effects of bad conditioning of the division of two flux densities in the proximity of zero crossings of either flux density. Because the saturation effect on the magnetic air gap flux density is dependent on the relative position of the air gap section to the stator teeth, an additional spatial order equal to the number of stator teeth N_S has to be considered in the permeance function. As the normal component of the magnetic flux density is continous between airgap and stator teeth, the eccenctric flux density amplitude is rescaled for each circumferential position α and time step t using the BH-Characteristic of the electrical stator steel.

$$B_\mathrm{Ecc}(\alpha, t) = B(H(B_\mathrm{Sym}(\alpha, t)) \cdot \lambda_\mathrm{Ecc}^*(\alpha, t)) \tag{8}$$

The change in phase of the magnetic flux density distribution is directly obtained from the unscaled, relative permeance function λ_Ecc. The radial and tangential force density σ_Rad and σ_Tan are calculated from the radial and tangential flux density components using the Maxwell stress tensor [8]:

$$\begin{aligned} \sigma_\mathrm{Rad} &= \frac{B_\mathrm{Rad}^2(\alpha, t) - B_\mathrm{Tan}^2(\alpha, t)}{2\mu_0} \\ \sigma_\mathrm{Tan} &= \frac{B_\mathrm{Rad}(\alpha, t) \cdot B_\mathrm{Tan}(\alpha, t)}{\mu_0} \end{aligned} \tag{9}$$

where μ_0 is the vacuum permeability. The electromagnetic forces for structural dynamic analysis are obtained by integration of the force densitiy over the stator teeth. As will be discussed in the next section, the calculated forces are applied to a finite amount of nodes on the surfaces of the stator teeth. Therefore, each tooth is divided into an amount of subsections correlating to the amount of model nodes on the mechanical mesh. For each timestep t the radial force on the jth node of the kth tooth is calculated to

$$F_{\mathrm{Rad},j,k}(t) = R_\mathrm{S} \cdot l \cdot \int_{\alpha_{\mathrm{T},k}+(j-1)\frac{W_\mathrm{T}}{n}}^{\alpha_{\mathrm{T},k}+j\frac{W_\mathrm{T}}{n}} \sigma_\mathrm{Rad}(\alpha, t)\,\mathrm{d}\alpha \tag{10}$$

where l is the axial length of the machine, $\alpha_{\mathrm{T},k}$ is the angular position of the beginning of the kth tooth, W_T is the angular width of a tooth and n_k is the amount of nodes on the kth tooth in the mechanical FEA model. The tangential forces on the stator teeth are calculated analogously.

C. Structrucal Dynamic Modeling

The general assumption of modal analysis is that the complex vibration mode of a structure can be described by a linear superposition of an infinite amount of singular, linearly independent vibration modes [9]. Each mode is characterized by its modal parameters, i.e its eigenfrequency, its eigenvector and the modal damping. These parameters are obtained by means of a numerical modal analysis. Each node in the mechanical FEA model possesses three translational degrees of freedom. As the differential equations of motion of the model nodes are coupled, obtaining the response of the structure to electromagnetic force loads is very time consuming. In order to decouple these differential equations of motion, the system is transformed into modal coordinates using principal component analysis. These linearly independent modes are modeled as separate spring-mass-damper systems as illustrated in figure 3 for the machine under investigation. When $\mathbf{z}$ is the modal matrix of the form

$$\mathbf{z} = \begin{pmatrix} z_{1,1} & z_{1,2} & \cdots & z_{1,m} \\ z_{2,1} & z_{2,2} & \cdots & z_{2,m} \\ \vdots & \vdots & \ddots & \vdots \\ z_{n,1} & z_{n,2} & \cdots & z_{n,m} \end{pmatrix} \tag{11}$$

then the degrees of freedom in principal coordinates x_p are calculated by

$$x_\mathrm{p} = \mathbf{z}^{-1} \cdot x \tag{12}$$

from the translational degrees of freedom x [10]. Each coloumn of the modal matrix represents a mode, each row represents the eigenvectors of the mode with respect to the degrees of freedom of the model nodes. Using the degrees of freedom in principal coordinates, a state space model of the form

$$\dot{x}(t) = \mathbf{A}x(t) + \mathbf{B}u(t) \tag{13}$$
$$y(t) = \mathbf{C}x(t) \tag{14}$$

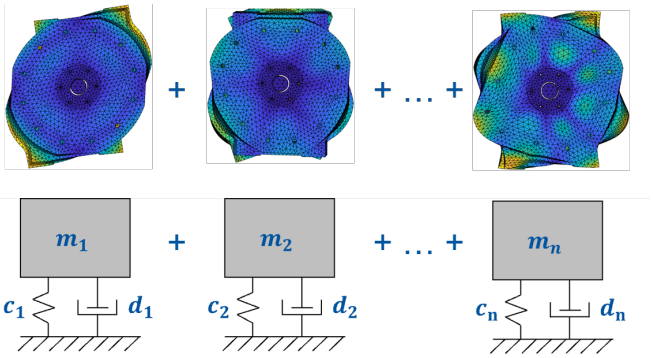

Fig. 3. Modal superposition in the machine under study.

is parameterized. For the example of a 2-degree-of-freedom system, the state space matrices $\mathbf{A}, \mathbf{B}, \mathbf{C}$ are

$$\mathbf{A} = \begin{bmatrix} 0 & 1 & 0 & 0 \\ -\omega_1^2 & -2\zeta_1\omega_1 & 0 & 0 \\ 0 & 0 & 0 & 1 \\ 0 & 0 & -\omega_2^2 & -2\zeta_2\omega_2 \end{bmatrix} \tag{15}$$
$$\mathbf{B} = \begin{bmatrix} 0 \\ F_{\mathrm{p},1} \\ 0 \\ F_{\mathrm{p},2} \end{bmatrix} \quad \mathbf{C} = \begin{bmatrix} z_{1,1} & 0 & z_{1,2} & 0 \\ 0 & z_{1,1} & 0 & z_{1,2} \\ z_{2,1} & 0 & z_{2,2} & 0 \\ 0 & z_{2,1} & 0 & z_{2,2} \end{bmatrix}$$

as presented in [10]. The parameters ω_n and ζ_n are the angular eigenfrequency and the modal damping of the nth mode, respectively. The principal forces F_p are obtained by multiplication of the transposed modal matrix with the vector of forces F on the respective degree of freedom:

$$F_\mathrm{p} = \mathbf{z}^\mathrm{T} F \tag{16}$$

The output y of the model yields the displacement and surface velocity of chosen nodes on the outer housing surface. In contrast to a full FEA analysis in the time domain, the computational effort is lowered by modal superposition with a finite number of modes. Only the vibration modes and the respective eigenvectors within the frequency range of the expected force excitation are considered. If n_m is the amount of vibrational modes within the frequency range, the state space problem is reduced to the solution of $2 \cdot n_m$ linearly independent first order differential equations.

III. Results

A. Magnetic Flux Density and Force Density Simulation

The flux density distribution in the airgap of the machine without rotor displacement is calculated using finite-element analysis. The chosen excitation represents the operation with the rated torque $T = 200$ Nm and the speed $n = 2000$ min^{-1} within the base speed range of the machine. The machine under study is a permanent-magnet excited synchronous machine with buried magnets, $2p = 8$ poles and $N_\mathrm{S} = 48$ stator slots. It is assumed that the effect of rotor eccentricity on the required stator current in order to produce equal torque is negligible.

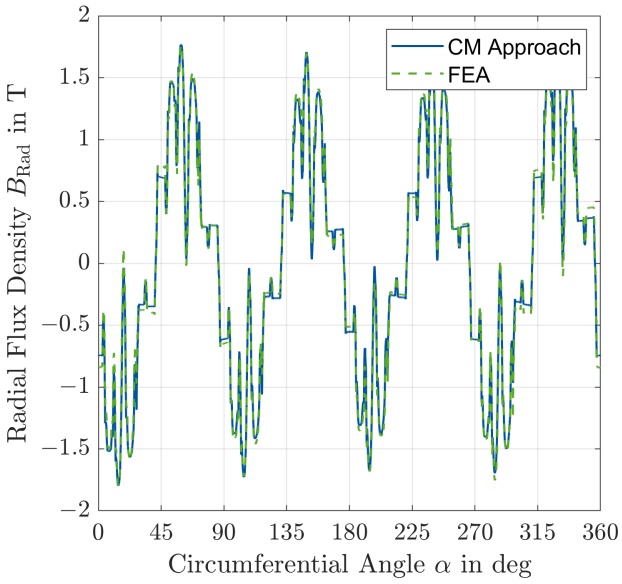

Fig. 4. Comparison of the radial component of the magnetic air gap flux density obtained from conformal mapping and FEA.

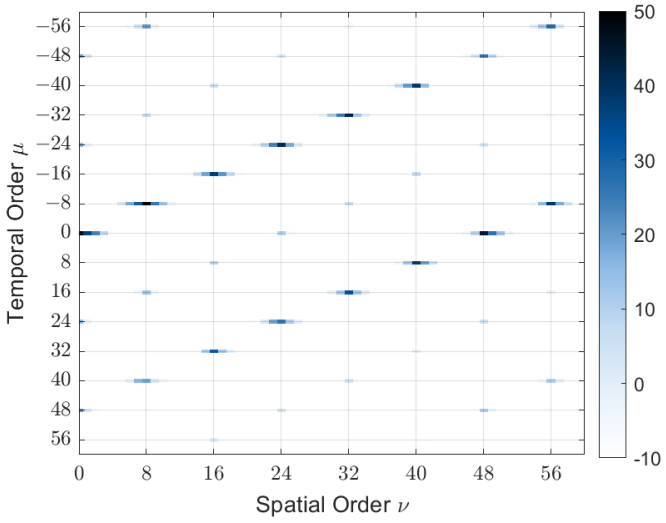

Fig. 5. Radial force density spectrum in dB re. 1 $\mathrm{kN/m^2}$ for a static eccentricity of $\frac{d_{\mathrm{Ecc}}}{\delta_{\mathrm{N}}} = 0.285$.

For validation purposes a static eccentricity of $d_{\mathrm{Ecc}} = 0.2\mathrm{mm}$ with its maximum at $\varphi = 0$ is investigated. This eccentricity equals 28.5% of the nominal airgap width δ_{N}.

In figure 4 the radial component of the magnetic air gap flux density obtained from the conformal mapping approach and FEA is illustrated for $t = 0$. The flux density amplitudes at the positions of maximum and minimum eccentricity match well. The approach used to rescale the analytically calculated, complex permeance function λ_{Ecc} only considers the decrease in amplitude due to saturation effects. Overall, the match between semi-analytical conformal mapping approach and FEA is sufficient for electromagnetic force calculation. In contrast, in order to compute the magnetic flux density distributions using only the FEA it is necessary to simulate a matrix of eccentricity amplitude and angular positions.

The magnetic flux densities obtained from the semi-analytical conformal mapping approach are used to calculate the magnetic force density as in (9). In figure 5 the radial force density spectrum for the case of $\frac{d_{\mathrm{Ecc}}}{\delta_{\mathrm{N}}} = 0.285$ is illustrated. The primary harmonic orders of force excitaion are multiples of the number of rotor poles and stator teeth, which are 8 and 48, respectively. Due to the static rotor eccentricity, additional force waves are excited. These force waves appear as harmonic side orders on the spatial axis of the force spectrum.

B. Structrucal Dynamic Model

To identify the modal parameters of the system a numerical modal analysis is conducted. In the scope of this work the stator force excitation and the resulting structural dynamic effects on the stator housing are considered. However, in order to correctly model the vibrational behaviour of the machine the structure is also taken into consideration for the modal analysis. Although the electromagnetic forces on the stator teeth are two dimensional, a three dimensional mechanical model is chosen. For the case of rotor displacements, which are not constant along the axial length of the machine, asymmetric loads are modeled by applying the two dimensional force excitations of the corresponding eccentricity to the nodes on the three dimensional mechanical mesh.

The resulting eigenfrequencies up to $6500\,\mathrm{Hz}$ are collected in Table I. Modes that occur in pairs with slightly different frequencies due to the rotational symmetry of the machine are only listed once as their averaged frequency but are regularly considered in structural dynamic simulation.

With the eigenvectors and eigenfrequencies from modal analysis the state space model is parametrized. The state space matrices **A** and **C** are implemented using the previously calculated eigenfrequencies and the resulting modal matrix z. These matrices are independent of the operating point of the machine

TABLE I
FLEXIBLE BODY EIGENFREQUENCIES OF THE MACHINE STRUCTURE OBTAINED FROM NUMERICAL MODAL ANALYSIS.

Mode No.	Frequency	Mode No.	Frequency
1	960.9 Hz	16	4770.4 Hz
2	1290.9 Hz	17	4798.3 Hz
3	1328.2 Hz	18	5087.6 Hz
4	1968.5 Hz	19	5246.0 Hz
5	2058.7 Hz	20	5357.7 Hz
6	2338.4 Hz	21	5422.2 Hz
7	2504.5 Hz	22	5537.9 Hz
8	3006.1 Hz	23	5626.3 Hz
9	3097.8 Hz	24	5843.6 Hz
10	3205.4 Hz	25	5896.5 Hz
11	3707.9 Hz	26	5956.8 Hz
12	3944.1 Hz	27	6077.8 Hz
13	3975.2 Hz	28	6301.2 Hz
14	4072.3 Hz	29	6408.3 Hz
15	4376.2 Hz	30	6459.1 Hz

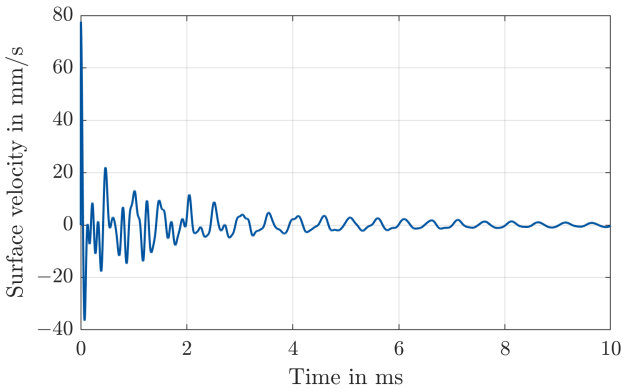

Fig. 6. Impulse response on the outer stator housing in the time domain.

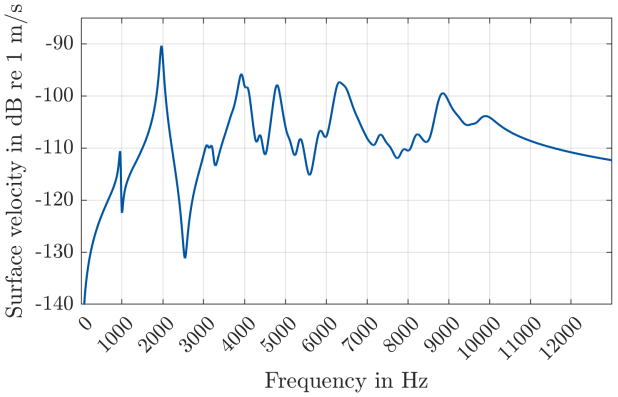

Fig. 7. Impulse response on the outer stator housing in the frequency domain.

and are constant in the scope of this work. The modal damping ratio, i.e. the percentage of critical damping, is assumed to be $\zeta_n = 0.02$. The state space matrix $\mathbf{B}$ represents the force excitation of the system. The force excitations used in this section are precalculated for symmetrical loads, constant static rotor eccentricity and static rotor eccentricity as a function of the axial rotor position. Hence, the rotor displacement has no influence on the runtime efficiency of the model.

The impulse response of the system is studied. A dirac-impulse is applied to a node on a stator tooth in radial direction.

In figure 6 and figure 7 the impulse response of the system is illustrated in the time and frequency domain, respectively. The surface velocity of a node on the stator housing is evaluated in radial direction. All peaks in the transfer function correspond to one of the eigenfrequencies of the system.

As a reference for the analysis of rotor displacements, the system behaviour for the case of $d_{\mathrm{Ecc}} = 0$ is studied and a run-up of the machine is simulated. A load torque of $T = 200\,\mathrm{Nm}$ is applied, which equals the force excitations presented in section III-A. In order to prevent system instability due to discontinuities in the force application, the force amplitude is ramped up in the first 0.1 seconds of the simulation. After this the machine is accelerated from $n = 100\ \mathrm{min}^{-1}$ to the rated

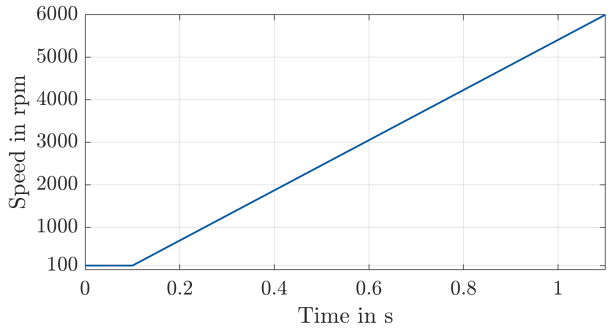

Fig. 8. Speed trajectory for the run-up of the machine.

speed $n = 6000\ \mathrm{min}^{-1}$ in one second. The time-speed profile of the run-up is shown in figure 8. The surface velocities and the outer stator housing nodes are studied. For the following evaluations, a node at half the axial length of the machine at $y = 0$ is chosen. Hence, the degree of freedom in x direction represents the surface velocity in radial orientation.

In figure 9 the frequency response of the system over the duration of the run-up is shown. The operating points of highest surface velocity can be matched with the input force excitations. The primary excitations marked with dotted lines correspond to the slot harmonics $\mu = 48$, $\mu = 96$ and $\mu = 144$. Generally, the structure is most susceptible to vibration at the eigenfrequencies $f_4 = 1968.5\,\mathrm{Hz}$ and $f_{17} = 4798.3\,\mathrm{Hz}$, which are highlighted as dashed lines in figure 9.

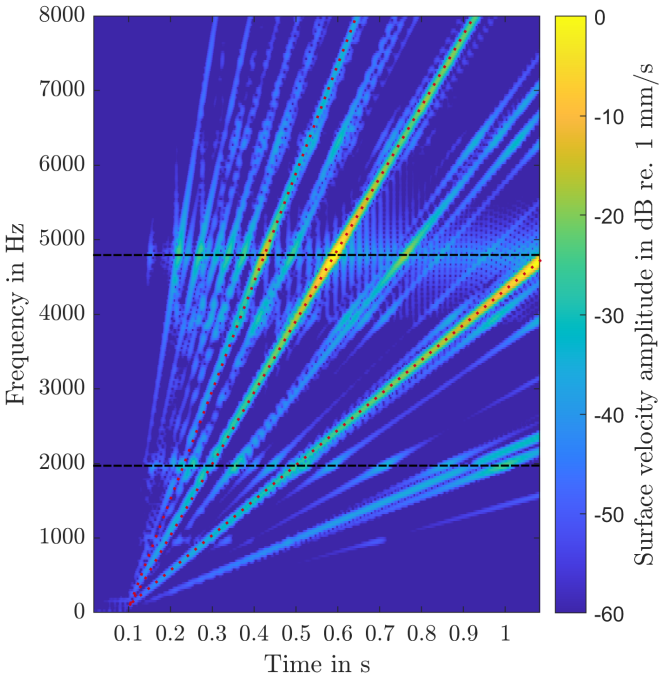

Fig. 9. Campbell-Diagram of a machine run-up from $n = 100\ \mathrm{min}^{-1}$ to $n = 6000\ \mathrm{min}^{-1}$ under symmetrical load.

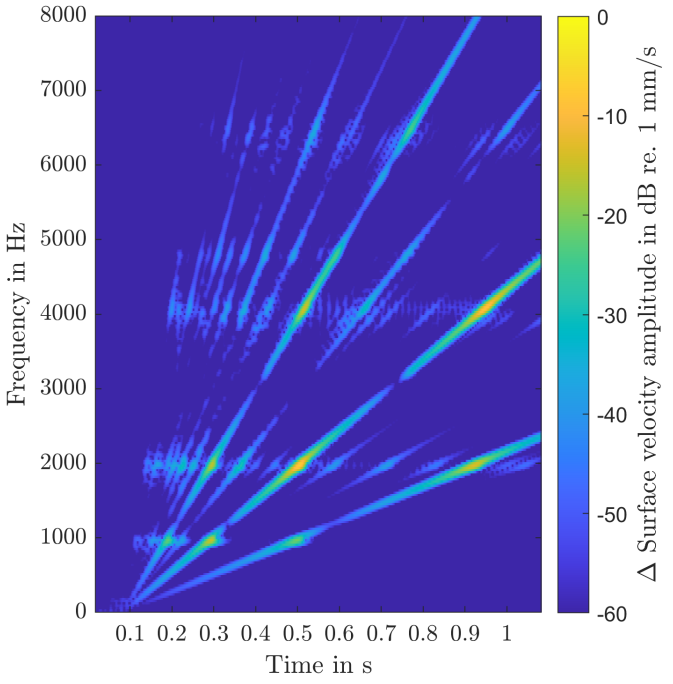

Fig. 10. Additionally excited vibrations due to the static eccentricity $\frac{d_{\mathrm{Ecc}}}{\delta_{\mathrm{N}}} = 0.285$ during run-up in comparison to symmetrical load.

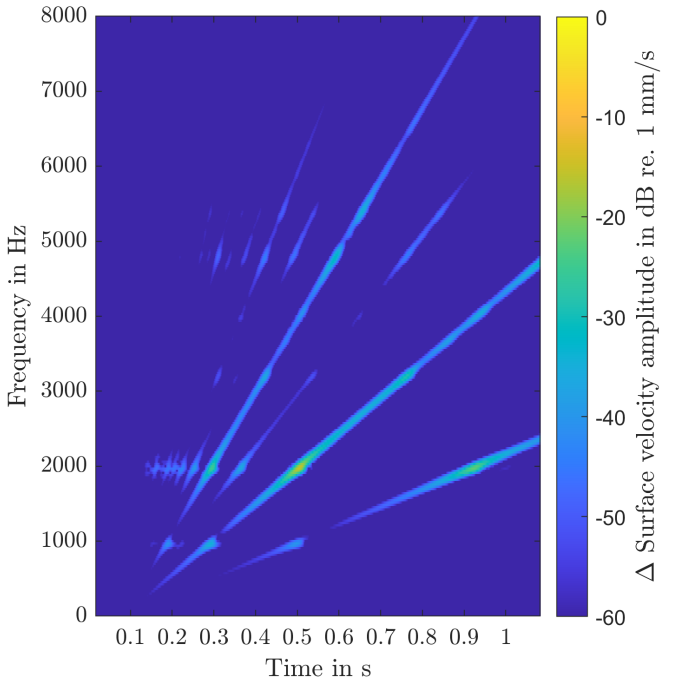

Fig. 11. Additionally excited vibrations due to the axially variable static eccentricity during run-up in comparison to symmetrical load.

The identical machine run-up is now performed with a uniform static eccentrcitiy of $\frac{d_{\mathrm{Ecc}}}{\delta_{\mathrm{N}}} = 0.285$ at $\varphi_{\mathrm{Ecc}} = 0$. The differences in amplitudes of surface velocity frequencies between eccentric simulation and the symmetrical reference are shown in figure 10. As shown in figure 5, the magnetic force excitation contains no additional frequency orders to due static eccentricity. The frequencies of the excited vibrations on the stator surface contain are identical to the symmetrical case. At the eigenfrequencies $f_5 = 1968.5\,\mathrm{Hz}$ and $f_{17} = 4798.3\,\mathrm{Hz}$ higher surface velocities are observed due to additional spatial orders in the slot harmonics of the machine. Furthermore, increased surface velocity amplitudes can be observed for the eigenfrequency $f_5 = 960.9\,\mathrm{Hz}$.

Static eccentricities with varying amplitudes along the axial length of the machine are investigated. For this, a tilted rotor shaft is considered. The rotor of the machine is shifted along the x-axis. The eccentricity amplitude and angle are a function of the axial position and vary from maximum eccentricity in x-direction ($\frac{d_{\mathrm{Ecc}}}{\delta_{\mathrm{N}}} = 0.285, \varphi_{\mathrm{Ecc}} = 0$) on one end of the rotor stack to maximum eccentricity in $-x$ direction ($\frac{d_{\mathrm{Ecc}}}{\delta_{\mathrm{N}}} = 0.285, \varphi_{\mathrm{Ecc}} = \pi$) on the other end. Depending on the z position of each node the force of the corresponding eccentricity amplitude is evaluated and applied to the node. The increase in surface velocity at the output node on the stator housing is illustrated in figure 11.

The vibration modes with increased amplitude match the ones seen in the case of uniform static eccentricity. The amplitude of vibrations at the observed point is lower, as the change in orientation of static eccentricity along the axial length of the machine partly cancels out additional excitation. It is expected that this configuration excites further three dimensional modes along the axial length of the machine. This effect will be analysed in future work.

IV. Conclusions and Future Work

In this paper, a time-efficient, semi-analytical methodology characterizing the vibrational behavior of permanent-magnet synchronous machines due to rotor misalignments is proposed. Symmetrical flux density distributions are obtained from the solution of a symmetrical finite element analysis. The effects of rotor eccentricity are taken into account by means of a conformal mapping approach. By transforming the domain of a regular annulus to an eccentric representation of rotor and stator, the complex relative permeance function is derived. By multiplication of the magnetic flux density distribution with the complex relative function the asymmetrical magnetic flux distributions are computed. The saturation state of the machine is considered and the magnetic flux density distributions are validated using FEA. Magnetic force density distributions are computed from the semi-analytical flux density. Additional orders excited due to eccentricity effects are discussed. Overall, instead performing a full finite-element simulation for each eccentricity amplitude and angle the resulting force excitations are calculated from one symmetrical FEA with sufficient accuracy. A numerical modal analysis is conducted and the eigenvectors and eigenfrequencies of the model are extracted and presented. The previously calculated force density excitations

are mapped to the nodes of the mechanical model. By applying the method of principal component analysis the degrees of freedom and excitation forces are transformed into principal coordinates. Force excitations are calculated for a reference without rotor eccentricity, a machine with statically eccentric rotor and a machine with a tilted rotor. A machine run-up is simulated and the results are presented. In both machines with non-uniform airgaps additional noise emissions due to side bands in the spatial stator slot harmonics are observed. Critical operation points in the run-up of the machine are identified. In future work, the effect of transient changes in the air gap shape of permanent-magnet synchronous machines will be studied. Dynamic eccentricities will be analysed and the interaction between unbalanced magnetic pull and transient change in air gap shape will be investigated.

REFERENCES

[1] J. F. Gieras, J. C. Lai, and C. Wang, *Noise of polyphase electric motors*, ser. Electrical and computer engineering. Boca Raton, FL: CRC/Taylor & Francis, 2006, vol. 129.

[2] D. G. Dorrell, M. Popescu, and D. M. Ionel, "Unbalanced magnetic pull due to asymmetry and low-level static rotor eccentricity in fractional-slot brushless permanent-magnet motors with surface-magnet and consequent-pole rotors," *IEEE Transactions on Magnetics*, vol. 46, no. 7, pp. 2675–2685, 2010.

[3] K. Jansen, A. Kern, C. Mülder, and K. Hameyer, "Study of magnetic force excitations in salient pole synchronous generators considering geometrical modifications by conformal mapping," *International Journal of Applied Electromagnetics and Mechanics*, vol. 69, no. 2, pp. 139–147, 2022.

[4] K. Boughrara, R. Ibtiouen, D. Zarko, O. Touhami, and A. Rezzoug, "Magnetic field analysis of external rotor permanent-magnet synchronous motors using conformal mapping," *IEEE Transactions on Magnetics*, vol. 46, no. 9, pp. 3684–3693, 2010.

[5] F. Boy and H. Hetzler, "A non-conformal mapping to avoid mesh deformation or remeshing in 2d fem-simulation of electrical machines with rotor eccentricity," in *Proceedings 2018 XIII International Conference on Electrical Machines (ICEM)*. Piscataway, NJ: IEEE, 2018, pp. 506–512.

[6] O. Florea, "A novel approach of the conformal mappings with applications in biotribology," *Analele Universitatii Ovidius Constanta - Seria Matematica*, vol. 23, no. 1, pp. 99–114, 2015.

[7] D. Zarko, D. Ban, and T. A. Lipo, "Analytical solution for electromagnetic torque in surface permanent-magnet motors using conformal mapping," *IEEE Transactions on Magnetics*, vol. 45, no. 7, pp. 2943–2954, 2009.

[8] M. Schröder, D. Franck, and K. Hameyer, "Analytical modeling of manufacturing tolerances for surface mounted permanent magnet synchronous machines," pp. 1138–1144, 2015.

[9] D. J. Ewins, *Modal testing: Theory, practice and application*, 2nd ed., ser. Engineering dynamics series. Hertfordshire: Research Studies Press, 2000, vol. 10.

[10] M. R. Hatch, *Vibration Simulation Using MATLAB and ANSYS*, 1st ed. Boca Raton, FL, USA: CRC Press, Inc., 2000.

V. BIOGRAPHIES

Kevin Jansen received his Master of Science degree in electrical engineering from RWTH Aachen University, Germany, in September 2019. Since March 2020 he has been working as a research associate at the Institute of Electrical Machines of RWTH Aachen University. His research focuses on the rotordynamics of electrical machines.

Marius Franck graduated with a Master of Science degree in mechanical engineering from RWTH Aachen University in 2018. Since August 2018, he has been working as a research assistant at the Institute of Electrical Machines at RWTH Aachen University. His research focuses on the acoustic and structural dynamic analysis of electrical machines.

Sebastian Mönninghoff received his Master of Science degree in mechanical engineering from RWTH Aachen University in 2019. Since January 2019 he has been working as a research assistent at the Institute of Electrical Machines at RWTH Aachen University. His research interest include the design of electric machines for traction and propulsion applications.

Kay Hameyer (IEEE M96 - SM99) received his M.Sc. degree in electrical engineering from the University of Hannover and his Ph.D. degree from the Berlin University of Technology, Germany. After his university studies he worked with the Robert Bosch GmbH in Stuttgart, Germany as a Design Engineer for permanent magnet servo motors and vehicle board net components. From 1996 to 2004 Dr. Hameyer was a full Professor for Numerical Field Computations and Electrical Machines with the KU Leuven in Belgium. Since 2004, he is full Professor and the director of the Institute of Electrical Machines (IEM) at RWTH Aachen University in Germany. In 2006 he was vice dean of the faculty and from 2007 to 2009 he was the dean of the faculty of Electrical Engineering and Information Technology of RWTH Aachen University. His research interests are numerical field computation and optimization, the design and controls of electrical machines, in particular permanent magnet excited machines and induction machines. For several years Dr. Hameyer's work is concerned with magnetically excited audible noise in electrical machines, the life time estimation of insulating systems and the characterization of ferro-magnetic materials. Dr. Hameyer is author of more than 250 journal publications, more than 700 international conference publications and author of 4 books. Dr. Hameyer is a member of VDE, IEEE senior member, fellow of the IET.